Improved nonlinear cross-polarized wave generation in cubic crystals by optimization of the crystal orientation

S. Kourtev,[1,*] N. Minkovski,[1] L. Canova,[2] A. Jullien,[2] O. Albert,[2] and S. M. Saltiel[1]

[1]*Sofia University "St. Kl. Ohridski", 5 J. Bourchier Boulevard, BG-1164 Sofia, Bulgaria*
[2]*Laboratoire d'Optique Appliquée, UMR 7639 CNRS, Ecole Polytechnique, ENSTA–Paristech, 91761 Palaiseau Cedex, France*
**Corresponding author: skourtev@phys.uni-sofia.bg*

Received February 10, 2009; revised April 15, 2009; accepted April 28, 2009; posted April 30, 2009 (Doc. ID 107420); published June 5, 2009

The efficiency of $\chi^{(3)}$-based cross-polarized wave generation in cubic crystals is investigated for different crystal orientations. It is shown that holographic-cut orientation is the optimal one. A 30% increase of the efficiency can be achieved with this orientation compared with the commonly used z-cut orientation. Another advantage of the holographic-cut crystal orientation is the weaker dependence of the optimal angle of input polarization on the input intensity. © 2009 Optical Society of America

OCIS codes: 190.7110, 190.4380, 320.5520, 320.7130.

1. INTRODUCTION

Cross-polarized wave (XPW) generation based on third-order nonlinear susceptibility [1] is a degenerated four-wave mixing process in nonlinear media that exhibit anisotropy of the real part of the $\chi^{(3)}$ tensor in which a linearly polarized input wave is converted to a perpendicularly polarized wave. In other words, having a strong input field $E_{\parallel}(\omega)$ in crystals with $\chi^{(3)}_{xxyy} \neq (1/3)\chi^{(3)}_{xxxx}$ it is possible to generate of a new field component $E_{\perp}(\omega)$ with polarization perpendicular to the input one due to the interaction symbolically presented as $\omega_{\perp} = \omega_{\parallel} + \omega_{\parallel} - \omega_{\parallel}$. In crystals without linear birefringence the phase-matching condition $k_{\perp} = k_{\parallel} + k_{\parallel} - k_{\parallel}$ is always fulfilled for the intensity range where the possible change in the wave vectors due to the contribution of the nonlinear index of refraction can be neglected.

While in some cases nonlinear optical modification of the polarization state is a drawback, there are new applications where the effect of XPW generation is very useful. For example, XPW generation has found its important application for contrast improvement of femtosecond optical pulses [2–4]. Recently, a nonlinear mirror based on XPW generation has been proposed [5]. Beam filtering and shaping have also been demonstrated [6]. Nonlinear media used in most cases are BaF_2 crystals, which are cubic ($m3m$ point group symmetry) crystals. In all cases BaF_2 crystals are oriented such that the light propagates along the z axis (z or [001] cut) of the crystal. In this paper we propose another orientation of the nonlinear crystal (NLC)—the so-called holographic cut, for which the nonlinear coupling coefficient that governs XPW generation maximizes. As XPW generation efficiency is of prime importance for practical use, we extensively compare z- and holographic-cut orientation for XPW-generation efficiency. The efficiency depends on the product [3]: nonlinearity $\times$ input intensity $\times$ crystal length. Besides intrinsic limitation of the energy efficiency that is due to the actual beam and pulse profiles, both the input intensity as well as the length of NLC are also limited by the optical damage threshold of the crystal and by self-action (self-focusing, self-diffraction) effects. Orientation dependence of nonlinear refraction [7–9] and two-photon absorption [9,10] in zinc-blende semiconductors have been investigated. Optimal NLC orientation for third-harmonic generation (THG) in cubic crystals has also been reported [11]. This motivated us to investigate orientation dependency of the above-mentioned XPW nonlinear coupling coefficient in order to maximize the XPW efficiency.

Crystals belonging to other than cubic symmetry groups, e.g., YVO_4 ($4/mmm$ point group symmetry) have also been used for XPW generation [12]. They, however, exhibit linear birefringence and can be used only in XPW devices oriented along their optical axes. Therefore, here we restrict our considerations to only cubic NLCs.

2. THEORETICAL ANALYSIS

We start our theoretical analysis with the following wave-propagation equation assuming a dielectric nonmagnetic nonlinear medium [13]. Dispersion effects will be neglected:

$$\Delta\vec{\mathcal{E}} - \frac{n^2}{c^2}\frac{\partial^2\vec{\mathcal{E}}}{\partial t^2} = \mu_0\frac{\partial^2\vec{P}^{\mathrm{NL}}}{\partial t^2},$$

where $\vec{\mathcal{E}}$ is the electric field, n is the linear index of refraction, c is the vacuum speed of light, μ_0 is vacuum permittivity, and $\vec{P}^{\mathrm{NL}}(\vec{\mathcal{E}}) = \varepsilon_0\chi^{(2)}\vec{\mathcal{E}}\vec{\mathcal{E}} + \varepsilon_0\chi^{(3)}\vec{\mathcal{E}}\vec{\mathcal{E}}\vec{\mathcal{E}} + \cdots$ is the nonlinear dielectric polarization. Only third-order susceptibility tensor $\chi^{(3)}$ is considered, thus

$$\vec{P}^{\mathrm{NL}}(\vec{\mathcal{E}}) = \varepsilon_0 \chi^{(3)} \vec{\mathcal{E}}\vec{\mathcal{E}}\vec{\mathcal{E}}.$$

In a Cartesian coordinate system for a plane wave traveling in the z direction we can write

$$\frac{\partial^2 \mathcal{E}_i}{\partial z^2} - \frac{n^2}{c^2}\frac{\partial^2 \mathcal{E}_i}{\partial t^2} = \varepsilon_0 \mu_0 \frac{\partial^2}{\partial t^2} \sum_{j,k,l} \chi^{(3)}_{ijkl} \mathcal{E}_j \mathcal{E}_k \mathcal{E}_l, \tag{1}$$

where indices i,j,k,l take x,y,z values. The plane wave for linearly isotropic medium ($k_x = k_y = k_z \equiv k$) in complex notation is written as

$$\mathcal{E}_i(z,t) = \frac{1}{2} E_i(z) \exp[-i(\omega t - kz)] + \frac{1}{2} E_i^*(z) \exp[+i(\omega t - kz)]. \tag{2}$$

From Eqs. (1) and (2), and using the slowly varying envelope approximation, the following system of ordinary differential equations can be derived:

$$\frac{\mathrm{d}E_i(z)}{\mathrm{d}z} = i\frac{2\pi}{8n\lambda} \sum_{j,k,l=x}^{z} \chi^{(3)}_{ijkl} [E_j(z)E_k(z)E_l^*(z) + E_j(z)E_k^*(z)E_l(z) + E_j^*(z)E_k(z)E_l(z)], \tag{3}$$

where the relation $2\pi/n\lambda = \varepsilon_0 \mu_0 \omega^2 / k$ is used. In the right-hand side of Eq. (3) terms that correspond to THG are omitted, since the process of THG is not phase matched. Estimated coherence length of the THG for BaF_2 at $\lambda = 620$ nm is 1.35 μm. With 1–2 mm thick BaF_2 crystals that are typically used for XPW generation the THG signal would be about 10^6 times weaker than the XPW signal.

$\chi^{(3)}_{ijkl}$ components are usually given in a coordinate system connected with crystalline axes, so we assume that (x,y,z) coincide with the corresponding crystalline axes. Components of the electric field of a wave that propagates in the k direction are, however, given in the other Cartesian coordinate system (A,B,k). In general (A,B,k) does not coincide with (x,y,z) basis. In the commonly investigated special case of a z-cut ([001] orientation) cubic NLC, k axis is along z or equivalent axis. Figure 1 defines the angles between the axes of the two coordinate systems: (φ,θ) define the crystallographic orientation, and β defines the angle of rotation of the input polarization around the propagation direction k. Further we shall refer to the wave E_A with polarization along the A axis as pump or fundamental wave (FW), and to the wave E_B polarized along the B axis as probe wave or XPW. Transformation of coordinates from (x,y,z) to (A,B,k) is given by

$$\begin{pmatrix} E_A \\ E_B \\ E_k \end{pmatrix} = \mathbf{T}(\varphi,\vartheta,\beta) \begin{pmatrix} E_x \\ E_y \\ E_z \end{pmatrix},$$

where the transformation matrix $\mathbf{T}(\varphi,\vartheta,\beta)$ is

$$\mathbf{T}(\varphi,\vartheta,\beta) = \begin{pmatrix} \cos\beta\cos\vartheta\cos\varphi - \sin\beta\sin\varphi & \cos\beta\cos\vartheta\sin\varphi + \sin\beta\cos\varphi & -\cos\beta\sin\vartheta \\ -\sin\beta\cos\vartheta\cos\varphi - \cos\beta\sin\varphi & -\sin\beta\cos\vartheta\sin\varphi + \cos\beta\cos\varphi & \sin\beta\sin\vartheta \\ \sin\vartheta\cos\varphi & \sin\vartheta\sin\varphi & \cos\vartheta \end{pmatrix}. \tag{4}$$

First, using the inverse matrix $\mathbf{T}^{-1}$, we find the components of E_A and E_B waves in (x,y,z) basis by

$$\begin{pmatrix} E_x \\ E_y \\ E_z \end{pmatrix} = \mathbf{T}^{-1}(\varphi,\vartheta,\beta) \begin{pmatrix} E_A \\ E_B \\ E_k \end{pmatrix}$$

and then we substitute them in the right-hand side of Eq. (3). There is no k component of the field thus $E_k = 0$ is set. Next, using Eq. (4) the derivatives in the left-hand side of Eq. (3) are combined to turn us back to the system connected with E_A and E_B waves. Finally, we obtain the following system of differential equations:

$$\frac{\mathrm{d}A(\zeta)}{\mathrm{d}\zeta} = i\gamma_1 AAA^* + i\gamma_2 AAB^* + 2i\gamma_2 ABA^* + 2i\gamma_3 ABB^* + i\gamma_3 BBA^* + i\gamma_4 BBB^*, \tag{5a}$$

$$\frac{\mathrm{d}B(\zeta)}{\mathrm{d}\zeta} = i\gamma_5 BBB^* + i\gamma_4 BBA^* + 2i\gamma_4 ABB^* + 2i\gamma_3 ABA^* + i\gamma_3 AAB^* + i\gamma_2 AAA^*. \tag{5b}$$

ζ is the longitudinal coordinate in the light propagation direction k. Polarization of the medium along the k axis does not generate electromagnetic wave; therefore, in Eq. (5) the expression for $\mathrm{d}E_k/\mathrm{d}\zeta$ is omitted. In Eq. (5) E_A and E_B are denoted simply as A and B, respectively, in order to correspond to the short version of this system of equa-

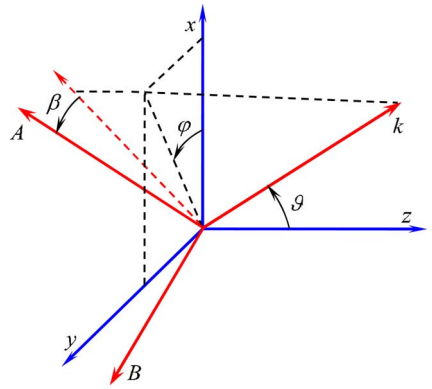

Fig. 1. (Color online) Definition of angles. (x,y,z)—basis of the nonlinear crystal; (A,B,k)—light propagation basis. The coordinate system (A,B,k) can be obtained from (x,y,z) by rotating (x,y,z) first around the z axis by an angle φ, then around the new y axis by ϑ, and finally by β around the k axis.

tions introduced in Ref. [14]. In the short version, z orientation (i.e., $\varphi=0$ and $\vartheta=0$) has been assumed, and because of the symmetry with respect to rotation around the z axis there are only three independent nonlinear coupling coefficients, since $\gamma_5=\gamma_1$ and $\gamma_4=-\gamma_2$. For arbitrary orientation of the nonlinear crystal such relations between coefficients are no longer valid. Instead, the following general relations for the coefficients in the full system (9) may be written:

$$\gamma_5(\beta,\varphi,\vartheta)=\gamma_1(\beta+\pi/2,\varphi,\vartheta), \tag{6a}$$

$$\gamma_4(\beta,\varphi,\vartheta)=-\gamma_2(\beta+\pi/2,\varphi,\vartheta). \tag{6b}$$

The above expressions (6) do not convey new physical information. They simply mean that rotating β by 90° B wave would become along $-A$, and A wave along the B axis. They could thus serve as a check for the correctness of derivation of γ coefficients.

Coefficients γ_1 and γ_5 are responsible for the self-phase modulation (SPM) while γ_2 and γ_4 govern the XPW conversion process from A to B and from B to A waves through the last terms in Eqs. (5b) and (5a), respectively. Note that generally self-phase modulation and XPW generation are not the same for the A and B waves except in the case of the commonly used z orientation. An interesting consequence of these nonequalities is that circular polarization will also be nonlinearly modified with holographic-cut crystals.

Besides the orientation γ coefficients in Eq. (5) depend also on the components of the $\chi^{(3)}$ tensor. We assume that the photon energy is below the half band gap and we neglect the two-photon absorption. In this case $\chi^{(3)}$ is a purely real tensor with only two independent components for crystals of $m3m$ cubic symmetry [11]: $\chi^{(3)}_{xxxx}$ and $\chi^{(3)}_{xxyy}$. The relation between them is usually defined [11] as $\sigma=(\chi^{(3)}_{xxxx}-3\chi^{(3)}_{xxyy})/\chi^{(3)}_{xxxx}$ and is referred to as the anisotropy of the $\chi^{(3)}$ tensor. Even in the relatively simple case of cubic crystals, explicit expressions for the γ coefficients as functions of β, φ, and ϑ are very lengthy analytical expressions. Here we prefer to take advantage of the transformation matrix $\mathbf{T}$ given in Eq. (4) and its inverse matrix $\mathbf{T}^{-1}$ to give more compact expressions for the γ coefficients:

$$\gamma_1=\gamma_0\sum_{j,k=1}^{3}[\delta_{jk}+(1-\delta_{jk})(1-\sigma)]T_{1j}T_{j1}^{-1}(T_{k1}^{-1})^2, \tag{7a}$$

$$\gamma_2=\gamma_0\sum_{j,k=1}^{3}[\delta_{jk}+(1-\delta_{jk})(1-\sigma)]T_{2j}T_{j1}^{-1}(T_{k1}^{-1})^2, \tag{7b}$$

$$\gamma_3=\gamma_0\sum_{j,k=1}^{3}\left\{\left[\delta_{jk}+\frac{2}{3}(1-\delta_{jk})(1-\sigma)\right]T_{j2}T_{k1}^{-1}T_{k2}^{-1}+\frac{1}{3}(1-\delta_{jk})(1-\sigma)T_{j1}^{-1}(T_{k2}^{-1})^2\right\}T_{1j}, \tag{7c}$$

$$\gamma_4=\gamma_0\sum_{j,k=1}^{3}[\delta_{jk}+(1-\delta_{jk})(1-\sigma)]T_{1j}T_{j2}^{-1}(T_{k2}^{-1})^2, \tag{7d}$$

$$\gamma_5=\gamma_0\sum_{j,k=1}^{3}[\delta_{jk}+(1-\delta_{jk})(1-\sigma)]T_{2j}T_{j2}^{-1}(T_{k2}^{-1})^2, \tag{7e}$$

where $\gamma_0=6\pi\chi^{(3)}_{xxxx}/8n\lambda$. δ_{jk} is the Kronecker delta symbol.

Investigation of Eq. (7b) shows that function $\gamma_2(\beta,\varphi,\vartheta)$, which is responsible for XPW generation, reaches its global maxima (with equal absolute values of γ_2) when $\varphi=2n\pi/4$ and $\vartheta=2(m+1)\pi/4$, or when $\varphi=2(n+1)\pi/4$ and $\vartheta=2m\pi/4$ where $m,n=0,1,\ldots$. This means that the light propagation direction k should lie in the (x,y), (x,z), or (y,z) plane just between (at 45°) the corresponding crystalline axes in order for the value of $|\gamma_2|$ to reach its maximum for certain values of the β angle. In this respect there are 12 equivalent optimal orientations of the NLC: [110], [$\bar{1}$10], [1$\bar{1}$0], [$\bar{1}\bar{1}$0], [101], [$\bar{1}$01], [10$\bar{1}$], [$\bar{1}$0$\bar{1}$], [011], [0$\bar{1}$1], [01$\bar{1}$], and [0$\bar{1}\bar{1}$], also known as holographic-cut orientations. For the eight equivalent to [111] propagation directions $\gamma_2=\gamma_4=0$ for any angle β and the orthogonal generation term is always zero regardless of the polarization state or orientation, and the medium shows isotropic behavior, which agrees with the results obtained in Refs. [7,8]. For these polarization preserving directions $\gamma_1=\gamma_5$ also holds.

3. NUMERICAL RESULTS

It has been shown [12,15] that, in the nondepleted regime, the efficiency of XPW generation is proportional to the squared XPW nonlinear coupling coefficient. The dependence of this coefficient, γ_2 in our case, on angle β is plotted in Fig. 2 for three orientations: the proposed most efficient one [101] (holographic cut), previously used [001] (z cut), and for the polarization preserving orientation [111]. In calculations $\sigma=-1.2$, a value that corresponds to the anisotropy of the BaF_2 [9] is used. As we see, the maximum absolute value of γ_2 for [101] cut is 12.22% greater than the maximum for z cut, and we may expect almost 26% increase in the XPW efficiency. This advantage does not depend on the particular choice of the value of σ since γ_2 depends linearly on σ.

Calculated values of the coefficients γ_1 and γ_5 that are responsible for self-phase modulation are presented in Fig. 3 for z- and holographic-cut crystals. These coefficients are driving the phase mismatch between input and XPW waves that impedes XPW generation.

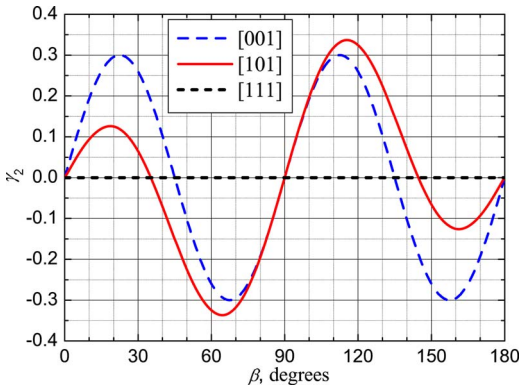

Fig. 2. (Color online) Calculated values of γ_2 normalized to γ_0 as function of angle β for different crystal orientations. $\sigma=-1.2$.

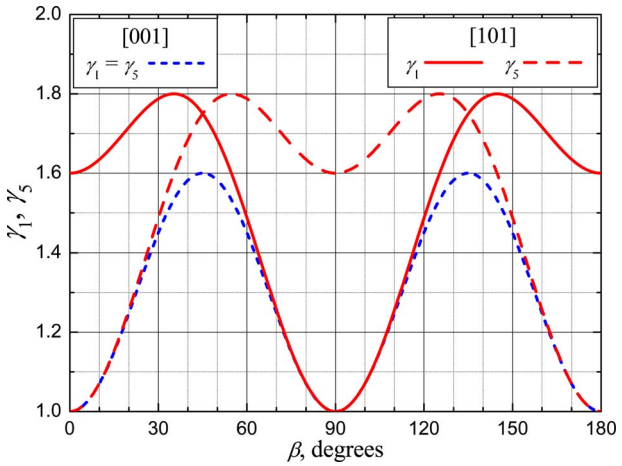

Fig. 3. (Color online) Calculated values of γ_1 and γ_5 normalized to γ_0 as functions of the angle β for z-cut ([001]) and holographic-cut ([101]) crystal orientations. $\sigma=-1.2$.

We numerically solve the system of differential Eqs. (5) in order to find the XPW-generation efficiency. In the case of plane-wave propagation the efficiency is defined as the ratio of the intensities of the XPW and the input fundamental wave. Calculated XPW efficiencies for the [101] and the [001] cuts (z cut) are shown in Fig. 4 along with phase shifts between the fundamental wave and the generated XPW. The dimensionless argument $S=\gamma_0|A_0|^2L$, where $A_0=A(\zeta=0)$ and L is the crystal length, is proportional to the product nonlinearity$\times$input intensity $\times$crystal length. The initial condition for the B wave is $B(0)=0$. β angles used in calculations correspond to the angles at which $|\gamma_2|$ is maximum for each cut (see Fig. 2). These angles are optimal for XPW generation at low input intensity. Figure 4 shows that, for [001] (z-cut) crystal, XPW efficiency reaches a maximum and then decreases when the phase shift between fundamental and XPW waves is getting higher than $\pi/2$. In the case of [101] (holographic-cut) crystal, the phase shift between fundamental and XPW waves stays below $\pi/2$ for almost twice higher S values. In this case the XPW efficiency reaches higher values.

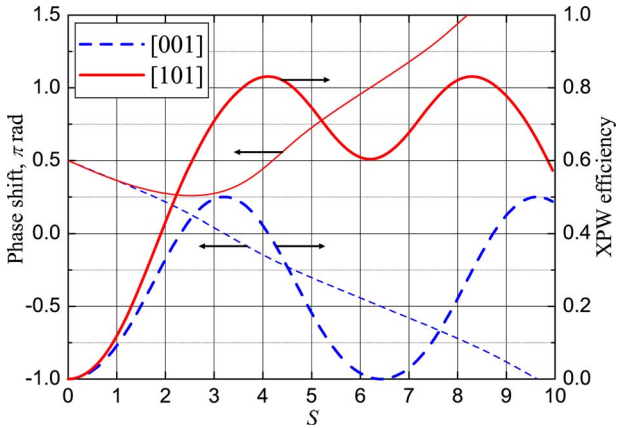

Fig. 4. (Color online) Numerically calculated plane-wave XPW efficiency (right scale, thick lines) and phase shift between the fundamental and XPW (left scale, thin lines) for [001] (z-cut) and [101] (holographic-cut) directions of light propagation. $\sigma=-1.2$; $\beta=22.5°$ for [001] and $\beta=115.5°$ for [101] orientation, respectively.

Computed β dependences of XPW efficiency for different values of S and assuming plane waves are plotted in Fig. 5. We notice that the four maxima [Fig. 5(a)] for [001] (z-cut) crystal are all equal. For any other crystal orientation including the holographic one [Fig. 5(b)] there are consecutive pairs of higher and lower maxima that is due the behavior of the nonlinear coupling coefficient (see Fig. 2).

It is known [12] that for z cut crystals the optimum β (at which generated XPW is maximum) depends on the input intensity. Indeed, from Fig. 5(a) we see that with increasing the input intensity up to the practical experimental limit for BaF_2 that corresponds to $S\approx5$ [16] the optimum β is shifted by as much as 13° for the z cut. From Fig. 5(b) we see that this shift does not exceed 5° for the higher maxima of holographic-cut crystal. At a slightly lower intensity the shift for [101] cut becomes very small, e.g., for $S=4$ the respective β shifts for z and [101] cuts are 10° and 2°. We may conclude that with holographic-cut orientation the optimum β is almost insensitive to changes in the intensity for the whole reasonable range of input intensities, which is in contrast to the strong dependence observed with the z cut. Furthermore, the curves for [101] cut [see Fig. 5(b)] remain quite wide even at high intensities. Therefore very precise alignment of β might not be necessary. In contrast, a precise β alignment is required for z cut due to the strong change in the XPW efficiency near the optimum β [see Fig. 5(a)].

The insensitivity of optimum β to input intensity for holographic-cut orientation is explained by the fact that, compared with the z-cut case, the phase-matching condi-

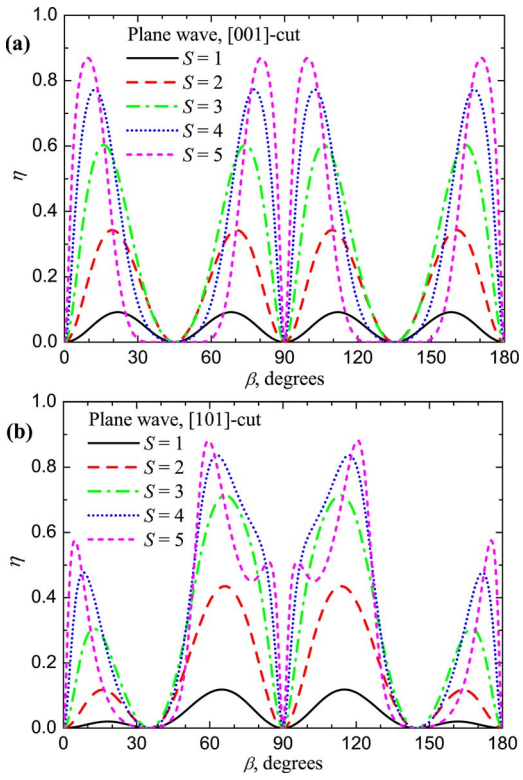

Fig. 5. (Color online) Plane-wave XPW efficiency η: (a) for [001] orientation, and (b) for [101] orientation as function of angle β for different input intensities. See text for definition of S. $\sigma=-1.2$.

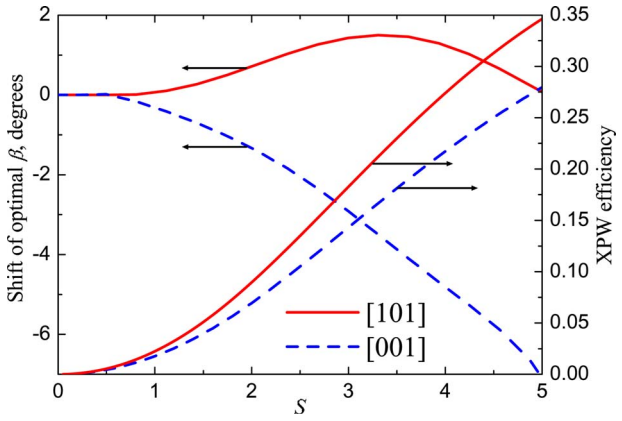

Fig. 6. (Color online) XPW efficiencies (right scale) for [001] and [101] orientations assuming Gaussian spatial and temporal profiles of the input beam. Angle β is always optimized for maximum efficiency. The shift of optimum β from its value β_0 for very low input intensity is also shown (left scale). β_0 is 22.5° for [001] and 64.5° for [101] orientation, respectively, and $\sigma=-1.2$.

tions for optimal phase shift between the two waves ($\pi/2$) are maintained over a bigger range of input intensities (see Fig. 4 left scale, thin lines). The deviation from the optimal phase shift for the holographic cut is less than $\pi/2$ up to $S=6$, while at the same conditions the deviation from the optimal phase shift for z cut is almost π. This insensitivity also means less distortions of the temporal and spatial shapes. This feature of the holographic-cut orientation is of importance in practice. It allows to obtain maximum XPW generation for a wide range of input intensities without any adjustment of the crystal orientation β. This is convenient in case the XPW setup is placed under vacuum to avoid SPM in air.

Efficiencies shown in Fig. 5 are obtained by direct solution of system (5) and are relevant to plane waves only. In a real experiment, finite beams formed from femtosecond pulses are used. The energy efficiency of the XPW process is obtained by taking into account the temporal and spatial shapes of the pulse. In the model the input beam is assumed to have Gaussian spatial and temporal profiles of the form $A(r,t,\zeta=0)=A_0\exp(-r^2)\exp(-t^2)$. Diffraction, dispersion, and self-focusing propagation effects are not included in the model. The results for XPW energy efficiencies for [001] and [101] cuts are shown in Fig. 6. It is seen that there is a solid advantage of the holographic cut over the z cut in terms of efficiency and β sensitivity. The ratio of [101] XPW efficiency to [001] XPW efficiency in the range $S=1,\ldots,5$ is between 1.24 and 1.29 reaching maximum for $S\approx 1.9$. On the same figure the shift of optimum β from its low-intensity value is also shown. Optimum β can be considered constant (less than 2° change) for [101] orientation compared with the strong variation calculated for [001] orientation.

4. EXPERIMENTS

The experimental setup is shown in Fig. 7. The NLCs used in the experiments are 2 mm thick z- and holographic-cut BaF_2 crystals. The BaF_2 samples are placed between two crossed Glan polarizers. Both the BaF_2 samples and the polarizers are uncoated. Input femtosecond pulses were focused with a lens into the BaF_2 crystals. Femtosecond laser source was a colliding-pulse mode-locked dye laser emitting in the visible (620 nm, 100 fs, 10 Hz).

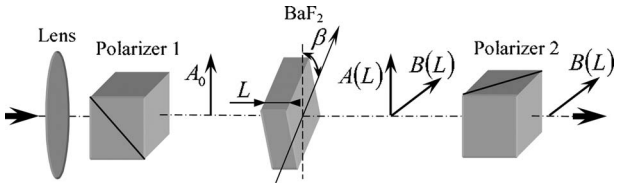

Fig. 7. Experimental setup.

Measured XPW conversion efficiencies are plotted in Fig. 8. The lens used was with $f=50$ cm. For the z-cut sample angle β was set to the optimal value for obtaining maximum efficiency in the range 40–50 μJ (detuned by 5° from the low-input optimum β thus giving about 25% higher efficiency in the said energy range). For the holographic-cut sample such optimization of angle β was not necessary. As can be seen from Fig. 8, conversion efficiency for both crystal orientations saturates at comparable levels but for the whole range of input energies where the conversion efficiency is not saturated the holographic-cut sample is more efficient. The XPW conversion efficiency saturates at a typical for single-crystal setup level [3,4,12] of approximately 10%. This saturation observed in experimental but not in the theoretical curves is obviously due to nonlinear effects that are not presently included in our model. Such effects might be, for example, change in the beam size due to self-focusing, self-diffraction, residual and induced chirp, and multiphoton absorption. Contributions of higher-order nonlinearities are also possible [17].

Straight lines in Fig. 8 are quadratic-law fits for the unsaturated efficiency. They correspond to approximately 1.45 times higher XPW generation efficiency for the holographic-cut sample compared with the z-cut one. Since it is preferable not to work in saturated regime when the XPW-generation effect is used for contrast filters the efficiency advantage of holographic cut is indeed useful.

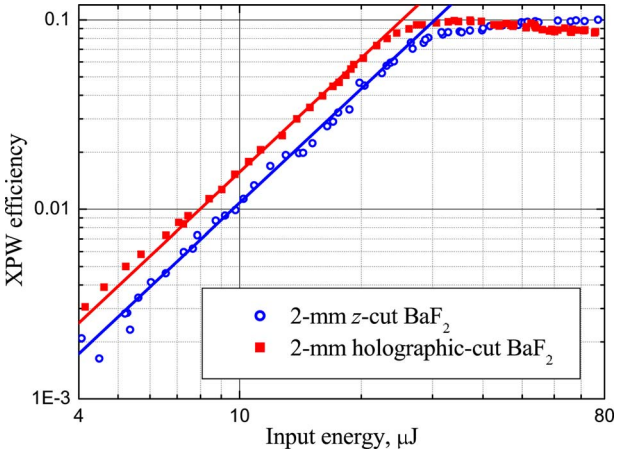

Fig. 8. (Color online) XPW generation efficiency for 2 mm BaF_2 holographic- and z-cut samples. Straight lines are quadratic-law fits.

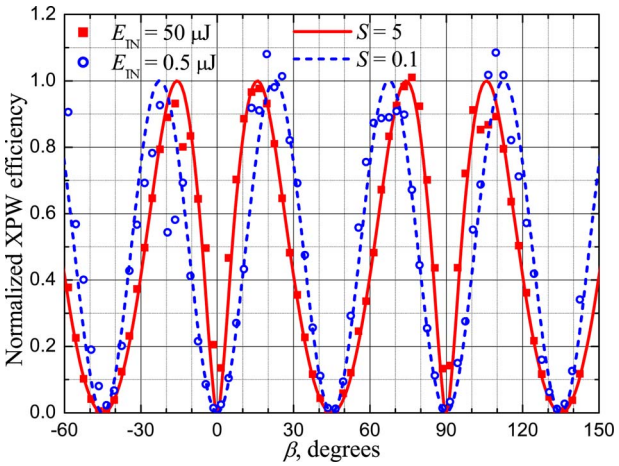

Fig. 9. (Color online) Experimental β dependencies (symbols) for 2 mm z-cut BaF_2. XPW generation efficiency is normalized to the average of all four maxima. Curves are numerically computed β dependences for different S and assuming Gaussian beam and pulse profiles. In calculations $\sigma=-1.2$ is used.

The β-dependence measurements for the z-cut sample are presented in Fig. 9. The theoretical curves in Fig. 9 are obtained by numerically solving system (5) assuming Gaussian shapes of the spatial and temporal profiles of the fundamental radiation. It is clearly seen that with increasing the input energy the optimum β is shifted by about 5°. The β-dependence measurements for the holographic-cut sample were performed with the second harmonic (310 nm) of the same dye laser and using a 140 mm focal-length silica lens for focusing the UV femtosecond pulses onto the BaF_2 crystal. The obtained results are shown in Fig. 10. The frequency-doubling medium was a 3 mm thick type I KDP crystal. The energy band gap of BaF_2 is wide enough, and no two-photon absorption that could influence the β-dependence behavior was registered. As seen from Fig. 10 the shift of the two smaller maxima is quite big (about 5°) but the positions of the two main maxima are almost insensitive to changes in the input intensity. This is consistent with the calculated behavior of the holographic-cut XPW.

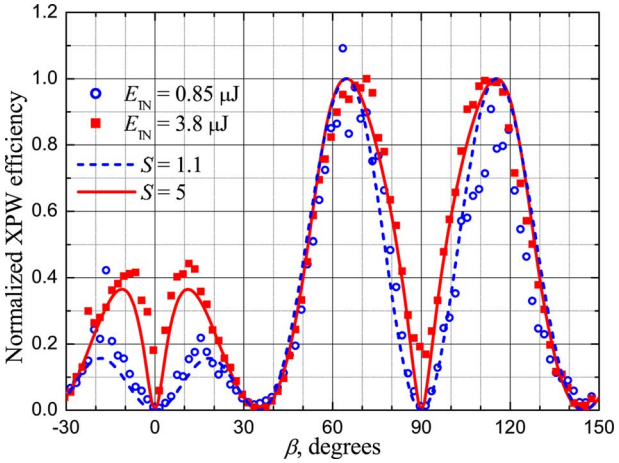

Fig. 10. (Color online) Experimental β dependencies (symbols) for 2 mm holographic-cut BaF_2. XPW generation efficiency is normalized to the average of the two higher maxima. Curves are numerically computed β dependences for different S and assuming Gaussian beam and pulse profiles. In calculations $\sigma=-1.2$ is used.

In Figs. 9 and 10, angles β, for which the XPW signal is minimal, correspond to the eigenpolarizations [8]. At these angles $\gamma_2=\gamma_4=0$ (see Fig. 2) and the orthogonal polarization term is zero. Their values in the range $0,\ldots,\pi$ for z-cut crystals are 0, $\pi/4$, $\pi/2$, $3\pi/4$, and π; while for holographic-cut crystals: 0, $\pi/2-\arctan\sqrt{2}$, $\pi/2$, $\pi/2+\arctan\sqrt{2}$, and π (see also Ref. [18]).

5. CONCLUSIONS

In conclusion, we show that the most efficient orientation for maximum XPW generation in cubic crystals is the holographic-cut orientation. We also demonstrate that when holographic-cut crystals are used for XPW generation, intensity dependent β compensation of the phase mismatch is not required. This feature makes the holographic cut easier to use for contrast filters in double chirped-pulse amplification schemes where the nonlinear crystal must be placed under vacuum. We believe that the use of the holographic-cut cubic crystals for XPW generation will lead to the design and construction of more efficient, reliable, and robust devices for temporal contrast improvement of femtosecond pulses.

The double-crystal scheme for XPW generation has been used [4,16] for increasing the efficiency of the single-crystal setup. The double-crystal scheme combined with crystal orientation optimization is a solution for further increase in the efficiency of the XPW generation process. Recently we reported [18] a record efficiency of 29% using two holographic-cut BaF_2 crystals in such a setup.

ACKNOWLEDGMENTS

The authors would like to acknowledge the partial support by the Consortium "LaserLab-Europe" through contract R||3-CT-2003-506350 and grant 212105 ("Extreme Light Infrastructure"), and also by the Bulgarian National Science Foundation through grant IRNI-17. S. Kourtev, N. Minkovski, and S. M. Saltiel thank the Laboratoire d'Optique Appliquée for their hospitality and support.

REFERENCES

1. Y. P. Svirko and N. I. Zheludev, *Polarization of Light in Nonlinear Optics* (Wiley, 1998).
2. A. Jullien, O. Albert, F. Burgy, G. Hamoniaux, J.-P. Rousseau, J.-P. Chambaret, F. Augé-Rochereau, G. Chériaux, J. Etchepare, N. Minkovski, and S. M. Saltiel, "10^{-10} temporal contrast for femtosecond ultraintense lasers by cross-polarized wave generation," Opt. Lett. **30**, 920–922 (2005).
3. A. Jullien, S. Kourtev, O. Albert, G. Chériaux, J. Etchepare, N. Minkovski, and S. M. Saltiel, "Highly efficient temporal cleaner for femtosecond pulses based on cross-polarized wave generation in a dual crystal scheme," Appl. Phys. B **84**, 409–414 (2006).
4. V. Chvykov, P. Rousseau, S. Reed, G. Kalinchenko, and V. Yanovsky, "Generation of 10^{11} contrast 50 TW laser pulses," Opt. Lett. **31**, 1456–1458 (2006).
5. S. Kourtev, N. Minkovski, S. M. Saltiel, A. Jullien, O. Albert, and J. Etchepare, "Nonlinear mirror based on cross-

polarized wave generation," Opt. Lett. **31**, 3143–3145 (2006).
6. S. Kourtev, N. Minkovski, L. Canova, O. Albert, A. Jullien, J. Etchepare, and S. M. Saltiel, "Nonlinear filtering and beam shaping with $\chi^{(3)}$ nonlinear polarization interferometer," Opt. Commun. **281**, 3375–3380 (2008).
7. D. C. Hutchings and B. S. Werrett, "Theory of the anisotropy of ultrafast nonlinear refraction in zinc-blende semiconductors," Phys. Rev. B **52**, 8150–8159 (1995).
8. D. C. Hutchings, J. S. Aitchison, and J. M. Arnold, "Nonlinear refractive coupling and vector solitons in anisotropic cubic media," J. Opt. Soc. Am. B **14**, 869–879 (1997).
9. M. Dabbicco, A. M. Fox, G. von Plessen, and J. F. Ryan, "Role of $\chi^{(3)}$ anisotropy in the generation of squeezed light in semiconductors," Phys. Rev. B **53**, 4479–4487 (1996).
10. M. D. Dvorak, W. A. Schroeder, D. R. Andersen, A. L. Smirl, and B. S. Werrett, "Measurement of the anisotropy of two-photon absorption coefficients in zinc-blende semiconductors," IEEE J. Quantum Electron. **30**, 256–268 (1994).
11. G. Petrocelli, E. Pichini, F. Scudieri, and S. Martellucci, "Anisotropic effects in the third-harmonic-generation process in cubic crystals," J. Opt. Soc. Am. B **10**, 918–923 (1993).
12. N. Minkovski, G. I. Petrov, S. M. Saltiel, O. Albert, and J. Etchepare, "Nonlinear polarization rotation and orthogonal polarization generation experienced in a single-beam configuration," J. Opt. Soc. Am. B **21**, 1659–1664 (2004).
13. A. Yariv and P. Yeh, *Optical Waves in Crystals* (Wiley, 1984).
14. A. Jullien, O. Albert, G. Chériaux, J. Etchepare, S. Kourtev, N. Minkovski, and S. M. Saltiel, "Nonlinear polarization rotation of elliptical light in cubic crystals, with application to cross-polarized wave generation," J. Opt. Soc. Am. B **22**, 2635–2641 (2005).
15. N. Minkovski, G. I. Petrov, S. M. Saltiel, O. Albert, and J. Etchepare, "Polarization rotation induced by cascaded third-order processes," Opt. Lett. **27**, 2025–2027 (2002).
16. A. Jullien, O. Albert, G. Chériaux, J. Etchepare, S. Kourtev, N. Minkovski, and S. M. Saltiel, "Two crystal arrangement to fight efficiency saturation in cross-polarized wave generation," Opt. Express **14**, 2760–2769 (2006).
17. V. M. Gordienko, P. M. Mikheev, and V. S. Syrtsov, "Nonlinear rotation of the polarization of the intense femtosecond laser radiation in BaF_2," Bull. Russ. Acad. Sci.: Phys. **71**, 122–125 (2007).
18. L. Canova, S. Kourtev, N. Minkovski, A. Jullien, R. Lopez-Martens, O. Albert, and S. M. Saltiel, "Efficient generation of cross-polarized femtosecond pulses in cubic crystals with holographic cut orientation," Appl. Phys. Lett. **92**, 231102 (2008).